Electron kinetic energy measurements from laser irradiation of clusters

E. Springate,* S. A. Aseyev, S. Zamith, and M. J. J. Vrakking
FOM Institute for Atomic and Molecular Physics, Kruislaan 407, 1098 SJ Amsterdam, The Netherlands
(Received 16 April 2003; published 3 November 2003)

We have measured electron kinetic energy spectra from the interaction of a low-density beam of noble-gas clusters with a high-intensity femtosecond laser pulse. Electron energies were measured both through their time of flight and through measurements of electron signals as a function of retarding voltages up to 7 kV. We have observed electrons with energies up to 6 keV and a sharp peak at an arrival time consistent with the detection of photons. The electrons had a broad angular distribution peaked along the polarization axis, while the sharp peak had an isotropic angular distribution. We attribute this sharp peak to uv, xuv, or x-ray photons formed as a result of the laser-cluster interaction and were unable to observe the two-lobed electron kinetic energy distribution reported by Shao *et al.* [Phys. Rev. Lett. **77**, 3343 (1996)] with any combination of the laser and cluster parameters used.

DOI: 10.1103/PhysRevA.68.053201 PACS number(s): 36.40.Gk, 52.50.Jm

INTRODUCTION

The interaction of clusters with high-intensity ultrashort laser pulses has been the subject of much research in recent years because the interaction is extremely energetic and displays many features that are not observed when intense femtosecond lasers interact with atoms, small molecules, or solid targets [1]. When a laser interacts with a beam of clusters at high density (by shooting directly under the gas jet from which the clusters are produced), a large yield of x rays from highly charged ions is produced [2–5]. Nearly all the laser radiation can be absorbed in the cluster gas [6]. The interaction is energetic enough that, when the clusters are formed from deuterium, nuclear fusion can occur, and a yield of more than 10^4 neutrons per laser shot has been observed from 100 mJ of laser energy [7]. Under these circumstances, the interaction is strongly affected by the clusters exploding into their neighbors and forming a low-density plasma. This results in x-ray emission which occurs on a much longer time scale (~nanoseconds) than the cluster explosion time scale [8]. Jets of extremely energetic (100 keV) electrons ejected along the laser propagation direction have also been observed and attributed to self-focusing and channeling of the laser pulse in the low-density plasma [9]. Space-charge effects preclude a measurement of the ion and electron energies from the exploding clusters under these conditions.

More information about the cluster explosion mechanism can be obtained by looking at the interaction of a low-density beam of clusters with an intense femtosecond laser. In the first reported measurement of the electron energy spectrum from clusters, Shao *et al.* [10] measured electron kinetic energies from Xe clusters with a mean size of 7000 atoms/cluster irradiated by a 150 fs pulse at an intensity of 1.3×10^{16} W cm^{-2}. An unusual two-lobed electron energy spectrum was measured, consisting of ''warm'' electrons with energies up to 2 keV ejected predominantly along the polarization axis and a sharp ''hot electron'' peak at 2.5 keV with an isotropic angular distribution with respect to the laser polarization.

These results were interpreted in the framework of the ''nanoplasma'' model developed by Ditmire *et al.* [8]. This model treats the cluster as a small, spherical plasma. Some atoms are ionized early on in the laser pulse, leading to an electron density high enough for the electric field in the cluster to be shielded from the external field. The cluster starts to expand slowly and as a result the electron density decreases. When the electron density in the cluster drops to three times the critical electron density (n_{crit}), the field inside the cluster is strongly enhanced, the electrons are heated to extremely high temperatures by inverse bremsstrahlung, and the cluster explodes under the combination of Coulomb and hydrodynamic pressure. In Ref. [10] the warm electron peak was attributed to electrons that leave the cluster early on in the laser pulse. Their angular distribution is peaked along the polarization axis because they are created predominantly through tunnel ionization and undergo a number of collisions before leaving the cluster. The ''hot'' electron peak was attributed to electrons that leave the cluster at the resonant heating point where the electron density n_e drops to $3n_{\mathrm{crit}}$.

More support for the nanoplasma model has been provided by measurements of ion kinetic energies. Ions with energies up to 1 MeV have been reported [11]. Measurements of ion kinetic energies as a function of cluster size [12], cluster ion species, laser pulse length, and intensity have been in good agreement with the model and support the idea that the interaction is dominated by the resonant heating point. They suggest that, in order to maximize the heating, the point where the electron density equals $3n_{\mathrm{crit}}$ should fall close to the peak of the laser pulse. For example, large clusters expand more slowly so there is an optimum cluster size for a given pulse length, and conversely an optimum pulse length for a given cluster size. Measurements of the angular distribution of the ions [13] and the energy as a function of charge state [14] have also given insights into the mechanism of the cluster explosion. However, the earlier interpretation of the electron energy spectrum [10] has recently been questioned by Kumarappan *et al.* [15,16], who found a correlation between the strength of the warm electron peak and the

*Present address: Blackett Laboratory, Imperial College London, London SW7 2BZ, United Kingdom.

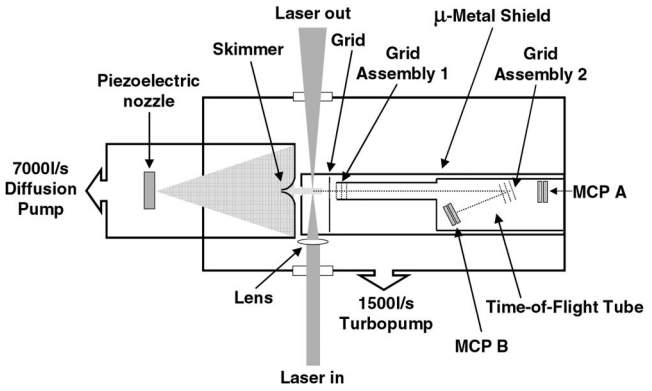

FIG. 1. Overview of the experimental arrangement. The noble-gas clusters are generated using a piezoelectric valve placed 20 or 30 cm before a skimmer that separates the source region from the experimental chamber. In the experimental chamber the clusters interact with the focused laser beam, and electrons formed in the explosion are detected either on MCP A, placed in the line of view of the experiment, or MCP B, which is reached by the electrons following a reflection from grid assembly 2. Using grid assembly 1 the detection can be restricted to electrons that have at least the kinetic energy corresponding to the stopping voltage on the central grid of this assembly.

ion energies as a function of pulse length, suggesting a common mechanism for the generation of both. These authors observed a warm electron peak extending to 5 keV that could be described well by a two-temperature thermal fit, and an additional signal implying a significant photon component in the signal or electrons with energies greater than this limit.

In this paper, we report measurements of electron kinetic energy spectra from laser interactions with Kr and Xe clusters with sizes from 10^4 to 10^6 atoms per cluster. The clusters were irradiated by laser pulses with lengths from 50 fs to 2 ps with focused intensities up to $\sim 10^{16}$ W cm^{-2}. We have observed warm electrons ejected predominantly along the laser polarization axis with energies as high as 6 keV under some conditions and a peak which, following a measurement of its arrival time, we attribute to photons, but we were unable to observe the hot electron peak reported by Shao *et al.* [10]. The electron energies follow similar trends to those observed in the ion energies, with a clear optimum pulse duration for a given cluster size being observed.

EXPERIMENT

Our experimental setup is shown in Fig. 1. The clusters were produced using a piezoelectric nozzle [17] with a 0.5 mm diameter orifice. With this nozzle, pressures up to 5 bar could be used. To extend the range of cluster sizes available in the experiments, we used both a conventional sonic nozzle and a conical nozzle with a 4° cone and a 20 mm length. The average size of the clusters produced can be estimated using the Hagena parameter [18,19]

$$\Gamma^* = k(d/\tan\alpha)^{0.85} T_0^{-2.2875}, \tag{1}$$

where d is the diameter of the nozzle (μm), T_0 is the temperature of the nozzle reservoir (K), α is the expansion half angle, and k is a gas-dependent constant that is equal to 5500 in the case of Xe. The Hagena parameter can be used to estimate the average cluster size according to

$$\langle N \rangle = 33(\Gamma^*/1000)^{2.35}. \tag{2}$$

In the present experiment, for a Xe nozzle backing pressure of 5 bar, we estimate the average cluster size to be 1.2×10^4 for the sonic nozzle ($\Gamma^* = 1.23 \times 10^4$) and 2.4×10^6 for the conical nozzle ($\Gamma^* = 1.18 \times 10^5$). Thus the average cluster size is up to 200 times higher with the conical nozzle than with the sonic nozzle.

The vacuum chamber containing the gas jet was pumped by an oil diffusion pump with a pumping speed of 7000 l/s. At a repetition rate of 50 Hz and a 5 bar backing pressure, the pressure in this chamber remained below 5×10^{-3} mbar. The gas jet was positioned 30 cm in front of a skimmer with a 0.5 mm orifice that separated the source chamber from the interaction chamber. The interaction chamber was evacuated to a pressure of 10^{-7} mbar by a 1500 l/s turbomolecular pump. The laser-cluster interaction took place 5 cm behind the skimmer. In the case of the sonic nozzle we estimate the gas density in the interaction region to be a factor of 3×10^6 lower than in the nozzle reservoir [18]. Using an average cluster size of 1.2×10^4 atoms/cluster, this leads to a predicted cluster density of about 3×10^9/cm^3. With the conical nozzle the cluster density is expected to be slightly lower. Therefore, when the laser is focused to a spot with a diameter of a few tens of micrometers, we expect to have several tens of clusters within the laser focus.

The laser was an amplified Ti:sapphire laser, producing 800 nm pulses at a 50 Hz repetition rate. The pulse energy on target was $\sim$10 mJ and the shortest pulse length obtained was 50 fs. The pulse length, which was calibrated using a single-shot autocorrelator, could be increased continuously up to 2 ps by changing the separation of the diffraction gratings inside the compressor. The intensity in the interaction region was calibrated by measuring the charge-state distribution in ionization of atomic Ne and monitoring the ratio of $^{20}Ne^{2+}$ (isotope abundance 90.5%) to $^{22}Ne^{+}$ (isotope abundance 9.2%) [20]. This led us to conclude that the peak intensity was $\sim 5 \times 10^{16}$ W/cm^2 at the shortest pulse duration, using $f/d = 7.5$ focusing optics. The prepulse on the nanosecond time scale was below 0.1%, as measured on a photodiode.

Electrons, ions, and photons produced in the interaction region were detected at the end of a 36 cm flight tube using a two-stage microchannel plate (labeled MCP A in Fig. 1). The front of this MCP was grounded and the anode signal was capacitively coupled to a digital oscilloscope. Two sets of three grids (labeled 1 and 2 in Fig. 1) were placed in the flight tube. In each set of grids, the outer two grids were grounded and a voltage could be applied to the central grid to provide a potential barrier to the electrons. The second set of grids was oriented at an angle of 8° with respect to the detector axis. This set of grids could be used to reflect the

electrons toward a second MCP (labeled MCP B in Fig. 1). The grids were made from Cu mesh (Buckbee-Mears MC17) with 70 wires per inch and 90% transmission. An additional grid mounted on a metal plate at the entrance to the flight tube screened the interaction region from the voltages on the MCP's and the connecting wires. The total transmission through the seven grids to MCP A was ~50%. The acceptance angle to MCP A was limited by the 2 cm diameter of the MCP to a solid angle of 8×10^{-4}.

Electron kinetic energy spectra could be obtained in three different ways. First, they could be obtained directly from the time-of-flight measurements using MCP A. Here the resolution was necessarily low, since the flight times were very short (for example, only 8.6 ns for 5 keV electrons) compared to the accuracy with which the time origin could be calibrated (±1 ns). However, as we will see later, these measurements played an important role in the qualitative interpretation of the features appearing in the time-of-flight measurements. Second, the spectra could be obtained by recording the integrated electron yield on MCP A as a function of voltage V_1 on grid 1 and differentiating the result. This procedure is similar to the one used by Shao *et al.* in Ref. [10]. Third, electron kinetic energy spectra could be obtained by using MCP B and recording the yield of electrons as a function of voltage V_1 on grid 1, while at the same time applying a voltage $V_1+\Delta$ to grid 2. In this case the signal recorded on MCP B corresponds to a slice out of the kinetic energy distribution where the kinetic energy lies between V_1 and $V_1+\Delta$. In practice the second (differentiation) and third (slicing) procedure gave similar results. Since the signals obtained with the slicing method were contaminated with overlapping signals resulting from electrons generated on grids 1 and 2 by photoelectron emission induced by photons produced in the clusters, the kinetic energy distributions presented in this paper were recorded exclusively with the differentiation method.

RESULTS

Figure 2(a) shows a number of time-of-flight traces recorded using the conical nozzle and Xe gas at a backing pressure of 5 bar (leading to an estimated cluster size of $\sim2.4\times10^6$ atoms/cluster), while applying different voltages to retarding grid assembly 1. The laser pulse duration was set to 400 fs, as this pulse duration maximized the production of high-kinetic-energy electrons. Delaying for now the discussion of the procedure used to define the time origin, Fig. 2(a) shows a sharp peak that appears after about 1 ns. This peak always appears in the same place, at a constant time delay of about 2.5 ns with respect to a fast photodiode signal measuring the arrival of the femtosecond ir pulse at the experimental chamber. We argue below that this peak is due to energetic photons. A small peak appears consistently ~6 ns after the first peak, with a height that is correlated to the height of the first peak. This second peak is due to ringing in the MCP assembly electronics. This was explicitly confirmed by measuring the time dependence for a single-particle event [also shown in Fig. 2(a)]. Following these first two peaks a broad lobe appears, where the low-energy components are removed

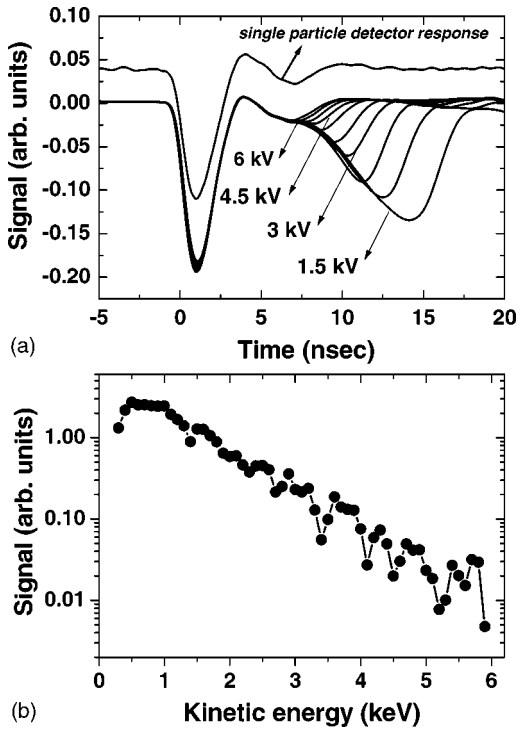

FIG. 2. (a) Series of time-of-flight traces for laser interactions with Xe clusters formed by expanding 5 bar Xe gas through a conical nozzle. The traces were recorded for different stopping voltages on the central grid of grid assembly 1, and the horizontal axis was calibrated using the procedure explained in the caption of Fig. 3. For successively higher voltages the low-energy tail of the electron time-of-flight distribution is removed, until no more electron signals are observed for stopping voltages above 6 kV. The sharp spike at a delay of 1.03 ns is attributed to the detection of photons produced as a result of the laser-cluster interaction. Also shown is a trace that shows the response of the detection system to a single ion or electron arriving on the detector. This trace illustrates that the bump that occurs at a delay of approximately 6 ns is due to electrical ringing. (b) Electron kinetic energy distribution derived from a series of time-of-flight measurements as shown in (a). The kinetic energy distribution is obtained by integrating the peak between 6 and 20 ns corresponding to the arrival of high-energy electrons and differentiating the result with respect to the energy.

when successively higher voltages are applied, until the lobe completely disappears for voltages below -6 kV. We conclude that this lobe reflects detection of electrons with energies up to 6 keV.

The reduction in the electron signals as a function of the applied voltage to retarding grid 1 can be used for calibration of the time axis. The flight time to the detector for electrons with a kinetic energy E_k scales as $t(E_k)=t_0+\alpha/\sqrt{E_k\ (\mathrm{eV})}$, where α is a constant that depends on the flight length and t_0 depends on the definition of the time origin. Using Fig. 2(a) we can estimate the flight time for electrons with an energy corresponding to the stopping voltage on grid assembly 1 as the time where, for a particular stopping voltage, the signal on the falling edge has dropped to 50% of the peak value. As shown in Fig. 3, this leads to a determination of $\alpha=629\pm7\ \mathrm{ns\,eV^{1/2}}$ and the conclusion that the first sharp peak oc-

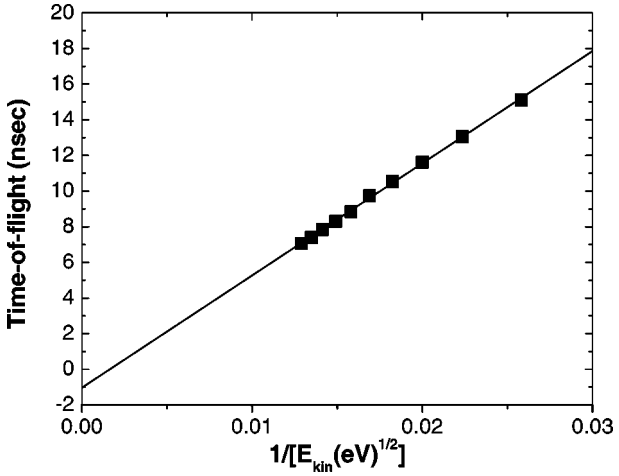

FIG. 3. Calibration of the time-of-flight axis and determination of time origin in experiments with Xe clusters formed by expanding 5 bar Xe gas through the conical nozzle. For a series of measurements with different stopping voltages on grid assembly 1, the time is plotted where the signal on the low-energy side of the electron peak has dropped to 50% of the maximum (taking the time origin as the appearance time of the sharp feature that is seen in all measurements). The solid line shows a fit to the arrival times obtained for stopping voltages between 1.5 and 6 kV, according to $t(E_k)=t_0+\alpha/\sqrt{E_k\,(\mathrm{eV})}$ and leads to a determination of $\alpha=629\pm7\ \mathrm{ns\,(eV)}^{1/2}$ and $t_0=1.03\pm0.12$ ns. This means that the sharp feature that we see at the beginning of each time-of-flight trace occurs at a delay of 1.03(12) ns with respect to the time origin and allows us to assign this peak to detection of photons formed as a result of the laser-cluster interaction.

curs 1.03 ± 0.12 ns after t_0, which is taken as the time origin from here on. Given this value of α, the flight time of electrons with a kinetic energy of 10^5 eV would be about 2 ns. In other words, if the first peak that is observed were to be an electron peak then the kinetic energy of these electrons would have to be *substantially higher* than 10^5 eV. Although electrons with energies up to 1 MeV ejected along the laser propagation axis have been observed from a much higher-density (6×10^{18} compared to 4×10^{13} cm^{-3}) cluster plasma [9], the mechanism relies on laser self-channeling, which requires a gas density or laser intensity several orders of magnitude higher than used in our experiments. The same experiment [9] also measured electrons with energies up to 100 keV emitted transverse to the laser propagation direction, which were attributed to resonant absorption at the critical density layer. However, we interpret the first peak in the flight-time measurement as the production of energetic photons (uv, xuv, or soft x-ray photons), with a photon energy exceeding the work function of the MCP detector. Given the 36 cm flight length of our instrument, we expect a photon flight time of 1.2 ns, which agrees very well with the observed position of the peak, taking into account the inaccuracies in the extraction of $t(E_k)$. We note that a peak at short (a few nanoseconds) arrival times has been observed previously [15,16] in electron flight-time measurements from clusters, but not identified conclusively as photons.

Our interpretation of the first peak in terms of photons is further supported by the fact that this peak is present under all conditions where we have clusters in the beam. As soon as we see electrons with higher kinetic energies than those obtained from the ionization of background gas, we also see this first peak, and always with exactly the same flight time. Importantly, the first peak is present *at the same flight time* even when the experimental conditions (gas expansion conditions, laser pulse duration, and focusing) are such that the electron kinetic energies are comparatively low. We are unable to make the first peak go away by applying voltages (up to -7 kV) to grid assembly 1. At slightly higher voltages, the onset of an electrical breakdown in the grid assembly (signaled by a rapid increase in the current drawn in the power supply providing the voltage for the grid assembly) leads to a significant current being drawn by the MCP. This results in a signal reduction as a result of a loss of gain of the MCP, and not through retardation of electrons with kinetic energies corresponding to the stopping voltage.

Figure 2(b) shows an electron energy spectrum obtained by differentiating the signal as a function of voltage using the same experimental conditions as in Fig. 2(a) (closed circles). In our experiments electrons are observed with energies up to at least 5 keV. In contrast with the results of Shao *et al.*, the electron energy distribution is quite smooth and there is no sign of a sharp peak of hot electrons in the distribution. This measurement has been repeated for a wide variety of experimental conditions with laser pulse lengths from 50 fs to 2 ps, using Ar, Kr, and Xe gas, using pulsed valve backing pressures from 1 to 5 bar, and using both the sonic and the conical nozzles. *In all cases* we have observed a single-peaked electron kinetic energy distribution, with the highest observed kinetic energies depending on the pressure, gas, and type of nozzle being used. Under none of these conditions has a sharp peak like that in the experiments of Shao *et al.* been observed. However, our measurement agrees with that of Kumarappan *et al.* [15], who reported a warm electron peak extending out to 5 keV and no hot electron peak in the 0–5 keV range.

The angular distributions of the two peaks in the time-of-flight trace were measured and are shown in Fig. 4. The electron signal has an angular distribution peaked along the laser polarization axis. The full width at half maximum (FWHM) of the distribution is $\sim40°$. The angular distribution of the photon peak is isotropic with respect to the laser polarization. We note that Shao *et al.* [10] measured a warm electron angular distribution peaked along the polarization axis with a FWHM of 60° and an isotropic distribution for the sharp hot electron peak.

For a given laser energy and cluster size there exists an optimum pulse length for the production of high-kinetic-energy electrons, as shown in Fig. 5. Figure 5(a) shows the photon and electron signals for three different pulse lengths at a fixed laser energy of 10 mJ, using the same cluster expansion conditions as Fig. 2. A stopping voltage of -2 kV was applied to grid 1 in this measurement. Case *A* corresponds to the shortest possible laser pulse in the experiment (approx 50 fs), where we observe that both the electron and photon signals are greatly reduced. Case *B* corresponds to a pulse length of ~500 fs. Here the hottest electrons are ob-

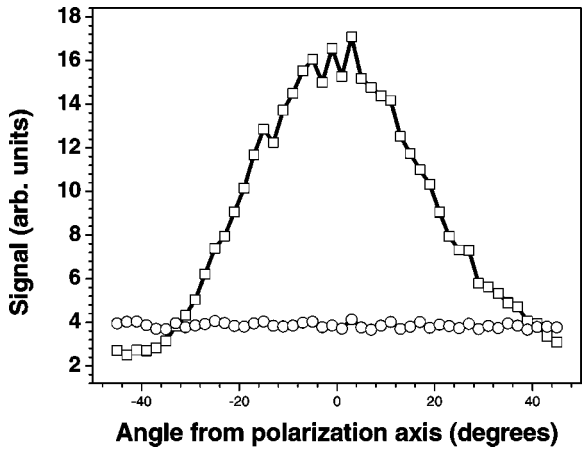

FIG. 4. Angular distribution of the photon peak (circles) and the hot electron peak (squares) obtained by recording time-of-flight traces for experiments with Xe clusters formed by expanding 5 bar Xe through the conical nozzle, as a function of the angle between the laser polarization axis and the detector time-of-flight axis.

served and significant numbers of electrons with energies above 2 keV are detected. Case *C* corresponds to a pulse length of about 2 ps. Here, no electrons above 2 keV are detected any longer, while the photon peak remains strong. The integrated photon and electron signals above 2 keV are shown in Fig. 5(b) as functions of compressor grating separation. It is apparent from this graph that the photon signal increases as the pulse length increases from 50 to ~500 fs, and then decreases only slowly as the pulse length is increased further. In contrast, the signal from electrons above 2 keV has a distinct optimum for 500 fs pulses and decreases sharply for longer pulse durations.

The trends in the electron kinetic energies correlate with similar trends that are observed in the ion kinetic energies. Figure 6 shows a number of time-of-flight traces, recorded using a 5 bar Kr expansion through the conical nozzle, for four different pulse durations. In (a), the segment in the time-of-flight measurement between -0.4 and 3 μs shows the arrival of highly charged Kr ions at detector MCP A. The fastest Kr ions are observed in measurement *B*, for a laser pulse duration of approximately 650 fs. Here, the first nonzero ion signal is observed after about 440 ns, which, according to the calibration of the time-of-flight axis, corresponds to a kinetic energy of about 300 keV. For shorter (measurement *A*) and longer (measurements *C* and *D*) laser pulses the ion kinetic energies are smaller. In the bottom frame, the segment in the time-of-flight measurement between -0.01 and 0.04 μs shows the arrival of fast electrons on the detector. As with the ion kinetic energies, the fastest electrons are observed in measurement *B*, for a pulse duration of 650 fs. In this measurement the first nonzero signal is observed after about 8.5 ns, which on the basis of the calibration of the electron flight times corresponds to an energy of about 5 keV.

DISCUSSION

In this paper we have presented observations of high-kinetic-energy electrons and photons from the irradiation of

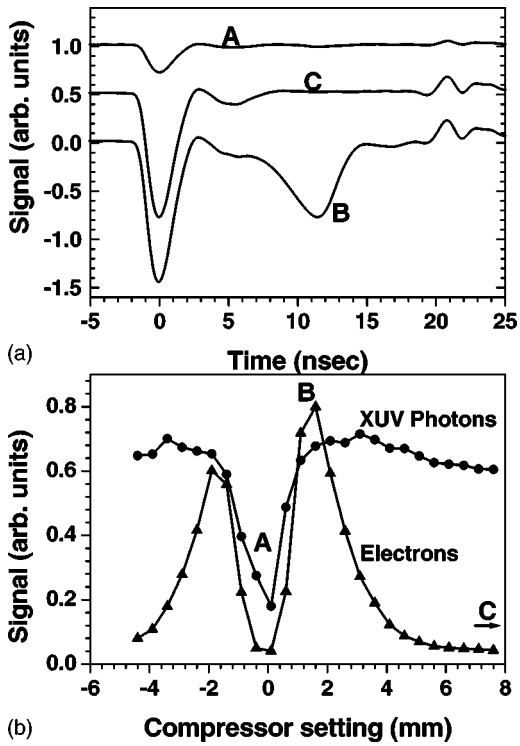

FIG. 5. (a) Observed time-of-flight traces for laser interactions with Xe clusters formed by expanding 5 bar Xe through the conical nozzle, obtained for three different settings of the compressor of the femtosecond laser system and using a 2 kV stopping voltage on grid assembly 1. Case *A* corresponds to the shortest possible laser pulse in the experiment (approx 50 fs), case *B* to a pulse length of ~500 fs, and case *C* to a pulse length of about 2 ps. (b) Integrated signal in the photon peak and the hot electron peak (recorded using a stopping voltage of 2 kV) as functions of the displacement of one of the two gratings in the compressor of the laser system with respect to the position where the shortest (50 fs) pulses are generated. The largest hot electron yield is observed for a grating displacement of about 2 mm, corresponding to a pulse duration of 500 fs.

noble-gas clusters with high-intensity laser pulses. The electrons had energies up to 6 keV under optimum conditions and were predominantly ejected along the laser polarization axis. The photons were observed whenever clusters were present in the molecular beam and were emitted isotropically. Under none of the conditions in our experiments have we seen evidence for the presence of a sharp, hot electron peak, whereas the photons observed by us were not previously observed in the experiment by Shao *et al.* [10,21].

We conclude that the first peak observed in our experiment corresponds to the detection of photons because (1) this peak appears, always at the same flight time, whenever clusters are present in the beam (i.e., even under conditions where the maximum kinetic energy of the warm electrons amounts to only a few hundred eV), and (2) a calibration of the flight time in our instrument shows that the first peak on the detector is consistent with photons moving at the speed of light or electrons with a kinetic energy of several hundred keV. Such electron kinetic energies are not realistic under the experimental conditions considered.

In the experiment of Shao *et al.*, the first peak was inter-

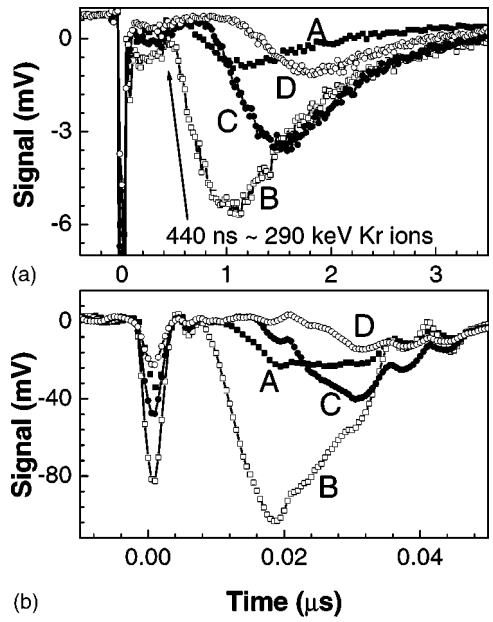

FIG. 6. (a) Ion time-of-flight distributions for the laser interactions with clusters formed by expanding 5 bar Kr through the conical nozzle. Case *A* corresponds to the shortest possible laser pulse in the experiment (approx 50 fs), case *B* to a pulse length of ~650 fs, case *C* to a pulse length of about 1.6 ps, and case *D* to a pulse length of about 2.6 ps. (b) Electron time-of-flight distributions recorded under the same conditions as in (a). A strong correlation between the formation of high-energy ions and of high-energy electrons is observed.

preted as electrons since the peak disappeared when a retarding voltage of -2.5 kV was applied to grids in the flight tube and also when a strong magnet was placed near the experimental apparatus [10,21]. Since the detector used in our experiments is surrounded by μ-metal shielding, measurements as a function of externally applied magnetic fields were not possible. The only way that we were able to remove the first peak was by applying excessively high voltages (-7 kV) to the grids, which caused a near breakdown of the detector. However, these high voltages were still more than one order of magnitude below the voltages that would be needed to block the detection of 100 keV electrons, if indeed we were to interpret the first peak in that way.

We should consider the possibility of differences in the experimental conditions that might lead to a situation where the hot electrons or photons would be observed only under a very narrow range of experimental conditions. To summarize, Ref. [10] used a Ti:sapphire laser operating at 780 nm with up to 40 mJ energy focused to 1×10^{16} W cm^{-2} at 150 fs. Clusters were formed when Xe at 4.5 bar expanded through a solenoid value with 600 μm diameter sonic nozzle and were skimmed after 20 cm with a 500 μm diameter skimmer. Reference [15] used an 806 nm Ti:sapphire laser with up to 12 mJ pulse energy in 100 fs focused to 1×10^{16} W cm^{-2}, and clusters were formed in the sonic expansion of 6 bar Xe through the 500 μm nozzle of a solenoid valve, followed by a skimmer with a 250 μm hole. Our experiments used an 800 nm Ti:sapphire laser with 10 mJ pulse energy in a 50 fs pulse focused to 5×10^{16} W cm^{-2} in 50 fs (or stretched up to a maximum of 2 ps, with an intensity of 1.7×10^{16} W cm^{-2} at 150 fs). We used a piezoelectric valve with 500 μm sonic or conical nozzle, a 500 μm skimmer 20 or 30 cm after the gas jet, and Xe, Kr, and Ar gases with pressures from 1 to 6 bar.

All three experiments are well above the predicted intensity threshold for the occurrence of the plasma resonance invoked for the explanation of the hot electron peak in Ref. [10], which according to the nanoplasma model occurs as soon as the laser intensity is greater than a few times 10^{14} W cm^{-2}, provided clusters of at least a few hundred atoms are present [12]. In this cluster size and intensity regime, ion energies greater than ~50 keV are then typically observed. These ions were clearly observed in our experiment, where we saw ions with kinetic energies as high as 300 keV from Kr clusters consisting of about 6×10^5 atoms (see Fig. 6) and in the experiment of Kumarappan *et al.* [15], who observed mean ion energies of 73 keV from Xe clusters.

The density of clusters in the interaction region can also affect the experimental measurement. If the cluster density is too high, then space-charge effects may prevent the hot electrons from leaving the cluster or may alter the kinetic energies of the detected electrons. In our experiment, the number of clusters in the focus is comparable to the numbers used in Ref. [10], since our gas jet had the same nozzle diameter and was located at a similar distance from the laser focus. Furthermore, we measured the electron energy spectrum with the gas jet either 20 or 30 cm away from the laser focus. The approximate factor of 2 reduction in the cluster density caused by pulling the jet back did not lead to any qualitative changes in the time-of-flight spectra.

Other possible differences between the experiments may be related to the residual chirp of the laser pulses used and the presence of prepulses or a pedestal underneath the laser pulse. We measured a noticeable asymmetry for positive and negative signs of the chirp applied to the pulse. This asymmetry is probably due to the slightly different pulse shapes that are obtained for increased and decreased compressor grating spacing (arising from the presence of a residual higher-order chirp and asymmetries in the spectrum of the pulse). Measurements of the x-ray yield from laser irradiation of a liquid jet [22] obtained with the same laser have shown a similar asymmetry with the sign of the chirp, and asymmetries in cluster heating have been observed in some experiments [23,24] but not in others [16]. While inverse bremsstrahlung heating rates of a cluster plasma may depend on the sign of the chirp of the laser pulse [24], the nanoplasma model predicts almost no dependence on the sign of the chirp [23].

As discussed in the Introduction, measurements of the ion energies as a function of cluster size, cluster ion species, laser pulse length and intensity, and pulse shape using shaped laser pulses [11,12,23,25] have all been in satisfactory agreement with the nanoplasma model, demonstrating the existence of an optimum laser pulse length for clusters of a particular size and ion species. This is strong evidence for the existence of resonant heating as described by the nanoplasma model. Figures 5(b) and 6 show that the warm electron signal also increases in size and energy in parallel with the ion

signal and clearly has an optimum for a particular pulse duration. The photon signal does not clearly show this optimum. The warm electrons observed in Ref. [10] were attributed to tunnel-ionized electrons leaving the cluster early in the laser pulse, while the hot electrons were expected to be the resonant contribution. This interpretation is clearly not borne out by our measurements, which suggest that it is the warm electrons (ejected predominantly along the laser polarization axis) that are most closely related to the resonance in heating. Kumarappan *et al.* [15] suggest that this is due to the polarization of the surface charge on the cluster, which lowers the Coulomb barrier over which electrons have to pass to leave the cluster along the laser polarization axis. The connection of the warm electrons with the resonance in heating, together with observed anisotropies in ion emission [13], suggest that the nanoplasma model (with its assumption that the cluster is a homogenous, isotropic plasma) does not fully describe the interaction.

In conclusion, we have reported the observation of both high-kinetic-energy electrons ejected predominantly along the laser polarization axis and photons ejected isotropically. These observations agree with recently published results of Kumarappan *et al.* [15] but disagree with the results of Shao *et al.* [10], and suggest that more experiments will be necessary in the future to determine more precisely the way in which the presence of a plasma resonance in the course of the explosion process manifests itself in the yield and the angular and energy distributions of the ejected electrons and photons.

ACKNOWLEDGMENTS

This work is part of the research program of the ''Stichting voor Fundamenteel Onderzoek der Materie (FOM),'' which is financially supported by the ''Nederlandse organisatie voor Wetenschappelijk Onderzoek (NWO).'' We acknowledge the technical assistance of A. Buijserd and R. Kemper and valuable discussions with J. Marangos, K. Mendham, and T. Ditmire. E.S. acknowledges the European Union for financial support. The research of S.Z. was supported by the COCOMO EU Network.

[1] For an extensive review, see V. P. Krainov and M. B. Smirnov, Phys. Rep. **370**, 237 (2002).
[2] A. McPherson, B. D. Thompson, A. B. Borisov, K. Boyer, and C. K. Rhodes, Nature (London) **370**, 631 (1994).
[3] T. Ditmire, T. Donnelly, R. W. Falcone, and M. D. Perry, Phys. Rev. Lett. **75**, 3122 (1995).
[4] T. Ditmire, R. A. Smith, R. S. Marjoribanks, G. Kulcsár, and M. H. R. Hutchinson, Appl. Phys. Lett. **71**, 166 (1997).
[5] S. Dobosz, M. Lezius, M. Schmidt, P. Meynadier, M. Perdrix, D. Normand, J.-P. Rozet, and D. Vernhet, Phys. Rev. A **56**, R2526 (1997).
[6] T. Ditmire, R. A. Smith, J. W. G. Tisch, and M. H. R. Hutchinson, Phys. Rev. Lett. **78**, 3121 (1997).
[7] T. Ditmire, J. Zweiback, V. P. Yanovsky, I. E. Cowan, G. Hays, and K. B. Wharton, Phys. Plasmas **7**, 1993 (2000).
[8] T. Ditmire, T. Donnelly, A. M. Rubenchik, R. W. Falcone, and M. D. Perry, Phys. Rev. A **53**, 3379 (1996).
[9] L. M. Chen, J. J. Park, K.-H. Hong, J. L. Kim, J. Zhang, and C. H. Nam, Phys. Rev. E **66**, 025402 (2002).
[10] Y. L. Shao, T. Ditmire, J. W. G. Tisch, E. Springate, J. P. Marangos, and M. H. R. Hutchinson, Phys. Rev. Lett. **77**, 3343 (1996).
[11] T. Ditmire, J. W. G. Tisch, E. Springate, M. B. Mason, N. Hay, R. A. Smith, J. Marangos, and M. H. R. Hutchinson, Nature (London) **386**, 54 (1997).
[12] E. Springate, N. Hay, J. W. G. Tisch, M. B. Mason, T. Ditmire, M. H. R. Hutchinson, and J. P. Marangos, Phys. Rev. A **61**, 063201 (2000).
[13] V. Kumarappan, M. Krishnamurthy, and D. Mathur, Phys. Rev. Lett. **87**, 085005 (2001).
[14] M. Lezius, S. Dobosz, D. Normand, and M. Schmidt, Phys. Rev. Lett. **80**, 261 (1998).
[15] V. Kumarappan, M. Krishnamurthy, and D. Mathur, Phys. Rev. A **66**, 033203 (2002).
[16] V. Kumarappan, M. Krishnamurthy, and D. Mathur, Phys. Rev. A **67**, 043204 (2003).
[17] D. Proch and T. Trickl, Rev. Sci. Instrum. **60**, 713 (1989).
[18] O. F. Hagena, Rev. Sci. Instrum. **63**, 2374 (1992).
[19] R. A. Smith, T. Ditmire, and J. W. G. Tisch, Rev. Sci. Instrum. **69**, 3798 (1998).
[20] V. R. Bhardwaj, S. A. Aseyev, M. Mehendale, G. L. Yudin, D. M. Villeneuve, D. M. Rayner, M. Yu. Ivanov, and P. B. Corkum, Phys. Rev. Lett. **86**, 3522 (2001).
[21] J. P. Marangos and T. Ditmire (private communication).
[22] E. Springate, H. L. Offerhaus, V. Kumarappan, and M. J. J. Vrakking (unpublished).
[23] K. J. Mendham, J. W. G. Tisch, M. B. Mason, N. Hay, and J. P. Marangos, Opt. Express **11**, 1357 (2003).
[24] Y. Fukuda, K. Yamakawa, Y. Akahane, M. Aoyama, N. Inoue, H. Ueda, and Y. Kishimoto, Phys. Rev. A **67**, 061201 (2003).
[25] S. Zamith, S. A. Aseyev, Y. Ni, and M. J. J. Vrakking (unpublished).